Surface roughness directed self-assembly of patchy particles into colloidal micelles

Daniela J. Kraft[a,1], Ran Ni[b], Frank Smallenburg[b], Michiel Hermes[b], Kisun Yoon[c], David A. Weitz[c], Alfons van Blaaderen[b], Jan Groenewold[a], Marjolein Dijkstra[b], and Willem K. Kegel[a]

[a]Van 't Hoff Laboratory for Physical and Colloid Chemistry, Debye Institute for NanoMaterials Science, Utrecht University, Padualaan 8, 3584 CH Utrecht, The Netherlands; [b]Soft Condensed Matter, Debye Institute for NanoMaterials Science, Utrecht University, Princetonplein 1, 3584 CC Utrecht, The Netherlands; and [c]Experimental Soft Condensed Matter Group, SEAS/Deptartment of Physics, Harvard University, Cambridge, MA 02138

Edited by Paul M. Chaikin, New York University, New York, NY, and approved April 16, 2012 (received for review October 14, 2011)

Colloidal particles with site-specific directional interactions, so called "patchy particles", are promising candidates for bottom-up assembly routes towards complex structures with rationally designed properties. Here we present an experimental realization of patchy colloidal particles based on material independent depletion interaction and surface roughness. Curved, smooth patches on rough colloids are shown to be exclusively attractive due to their different overlap volumes. We discuss in detail the case of colloids with one patch that serves as a model for molecular surfactants both with respect to their geometry and their interactions. These one-patch particles assemble into clusters that resemble surfactant micelles with the smooth and attractive sides of the colloids located at the interior. We term these clusters "colloidal micelles". Direct Monte Carlo simulations starting from a homogeneous state give rise to cluster size distributions that are in good agreement with those found in experiments. Important differences with surfactant micelles originate from the colloidal character of our model system and are investigated by simulations and addressed theoretically. Our new "patchy" model system opens up the possibility for self-assembly studies into finite-sized superstructures as well as crystals with as of yet inaccessible structures.

anisotropic colloids | depletion interactions | Monte-Carlo simulations

Nature has mastered the self-assembly of simple basic subunits into complex, functional structures with outstanding precision. Examples include biological membranes and viruses, which exhibit excellent control over the assembled structures with respect to their functionalities, shapes or sizes. However, the interactions between the building blocks, in the case of viruses, the protein subunits, are often complex and it remains challenging to identify the key elements for guiding and controlling the self-assembling process. By mimicking such self-assembly processes on a colloidal scale, insights into the paramount elements that control the assembly can be obtained in situ and applied to build up superstructures with new and desirable properties.

Colloidal particles with site-specific directional interactions, so called "patchy particles", are promising candidates for bottom-up assembly routes towards such complex structures with rationally designed properties (1–3). The size and geometry of the patches together with the shape of the interparticle potential are expected to determine the formed structures and phases, which may range from empty liquids (4) and crystals (5–7) to finite-sized clusters (1, 2, 8–11), and lead to novel collective behavior (12).

Recent experimental approaches to assemble colloidal particles at specific sites include hydrophobic-hydrophilic interactions (6, 7, 13–15), and lock-and-key recognition mechanisms (16). With a wide variability of colloidal shapes available today, the ultimate challenge is to identify general methods to render specific areas of the colloids attractive or repulsive, while not depending on a specific choice of material or surface chemistry (17). Ideally, the attraction strength and range is tunable and interactions are reversible to allow the formation of equilibrium structures.

Results and Discussion

Our approach to achieve patchy particles employs depletion interactions between particles that have locally different surface roughness, as for example shown in Fig. 1*A*. Depletion attraction arises in dispersions of colloidal particles when a second, smaller type of non-adsorbing colloid or macromolecule, also termed depletant, is introduced in the suspension (18–20). The center of mass of the depletant cannot approach the surface of the larger colloidal particles closer than its radius r_p, restricting the volume available to it (see Fig. 1*B*). The volume around the colloidal particles unavailable to the depletant is called the exclusion volume.

When the surfaces of two large colloids come closer together than the diameter of the depletant, $2r_p$, their exclusion volumes overlap and the volume accessible to the depletant increases by the amount of this overlap volume ΔV. Hence the entropy of the depletant, increases, and an effective attractive potential is induced between the two larger colloids (18–20). The depletion potential is roughly proportional to the number density of the depletant ρ_p and the overlap volume ΔV as $u_{\mathrm{AO}} = -\rho_p\ k_{\mathrm{B}}T\ \Delta V$. Here, k_{B} is Boltzmann's constant and T is the temperature. Smooth surfaces have larger overlap volumes than incommensurate rough surfaces, and thus are more strongly attracted towards each other. Experimentally, this effect was first described for plates and cylinders by Stroock and co-workers (21, 22) and Mason and co-workers (23, 24) and exploited to achieve side-specific attraction between platelets by introducing roughness on only one of the two sides (24). Roughness was also shown to suppress the depletion driven attraction between mesoscopic bilayers consisting of colloidal rods (25).

We employ this surface roughness specific depletion interaction to create particles with distinct attractive sites on curved surfaces. Our patchy particles are anisotropic polystyrene dimers that consist of one rough and one smooth sphere as shown in Fig. 1*A*. For this, we prepared rough cross-linked polystyrene particles from linear polystyrene spheres by seeded emulsion polymerization. During polymerization, roughness is achieved through adsorption of smaller polystyrene spheres at the surface. Using these particles in a seeded emulsion polymerization yields rough spheres with a smooth protrusion after phase separation (26–29). The synthesis protocol is sketched schematically in Fig. S1. The final particles with a small smooth patch shown in the Fig. 1*A* (*Left*) have a protrusion radius of 1.11 μm (smooth

Author contributions: D.J.K., A.v.B., M.D., and W.K.K. designed research; D.J.K., R.N., F.S., M.H., K.Y., D.A.W., J.G., M.D., and W.K.K. performed research; D.J.K. and W.K.K. analyzed data; and D.J.K. and W.K.K. wrote the paper.

The authors declare no conflict of interest.

This article is a PNAS Direct Submission.

Freely available online through the PNAS open access option.

[1]To whom correspondence should be addressed at the present address: Center for Soft Matter Research, Department of Physics, New York University, 4 Washington Place, New York, NY 10003. E-mail: d.j.kraft@uu.nl.

This article contains supporting information online at www.pnas.org/lookup/suppl/doi:10.1073/pnas.1116820109/-/DCSupplemental.

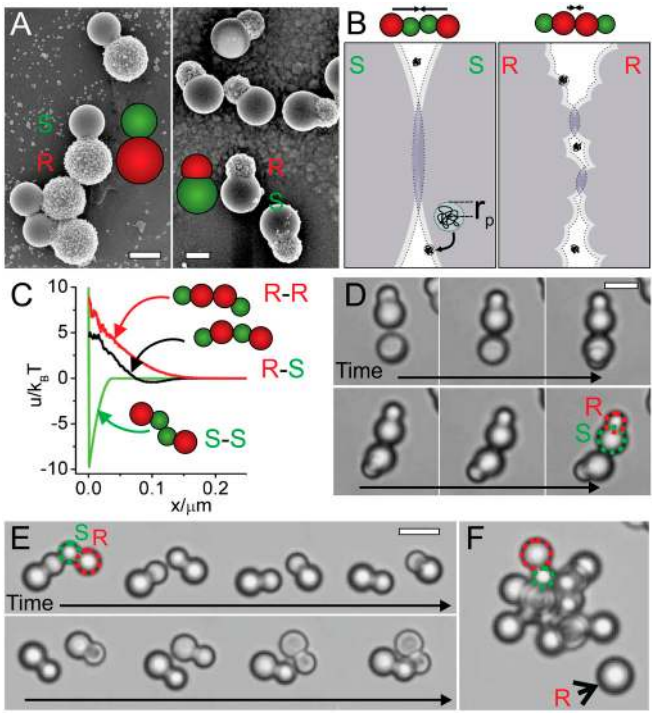

Fig. 1. *Patchy particles by roughness specific depletion interactions.* (*A*) Colloidal model systems consisting of one sphere with a smooth and one sphere with a rough surface. Scale bars are 2 μm. (*B*) In the presence of small depletants (here depicted as polymers with radius r_p) the colloidal particles are surrounded by a layer inaccessible to the depletant (dotted line). If colloidal particles approach such that their excluded volumes overlap, the depletant gains entropy, which results in a net attraction between the colloids. The resulting depletion attraction is proportional to the overlapping excluded volume (blue regions). For two rough spheres the overlap volume is significantly reduced compared to that for smooth particles. Small arrows represent the effective forces on both colloids. (*C*) Depletion potentials obtained from simulations between two smooth, two rough and one smooth and one rough side of our colloids, and polymer of size $r_p = 19$ nm ($\rho_p = 0.038\ \rho_{overlap}$) as a function of the distance x between the surfaces of the colloids (for details, see *SI Text*). (*D*) Snapshots from a movie showing the breaking of a bond between the smooth sides of two particles and later reformation of the bond. Dextran polymer with radius $r_p = 19$ nm was used at a concentration of $\rho_p = 0.4\ \rho_{overlap}$. Scale bar is 5 μm. (*E*) Rough spheres as indicated by the black arrow are left out of the colloidal micelles formed from the particles with one attractive patch. (*F*) Bond formation between the larger smooth sides of two particles and subsequent rearrangement due to the flexible bond (Dextran polymer, $r_p = 8.9$ nm, $\rho_p = 0.20\ \rho_{overlap}$, 0 mM NaCl). Scale bar is 5 μm.

side, colored in green, polydispersity (pd) 2.9%), seed radius of 1.46 μm (rough side, colored in red, pd 2.2%) and are 4.9 μm in length (pd 2.9%). SEM images show that small particles of 185 nm (pd 16%) are partially immersed into the seed particle (Fig. S1*B*) effectively creating roughness on a scale of only a hemisphere of the secondary nucleated particles as depicted schematically in Fig. 1*B*. The protrusion size is continuously tunable by adjusting the monomer concentration during synthesis (26–29). Colloidal particles with protrusions larger than the seed particles (protrusion radius 1.66 μm, pd 3.4 %; seed particle radius 1.2 μm, pd 4.2%; roughness diameter 182 nm, pd 22%; long axis 4.70 μm, pd 3.2%) were synthesized as well to demonstrate the effect of particle geometry on the assembled structures (Fig. 1*A*, *Right*).

We calculated the effective pair potential of spherical particles between two smooth, two rough, and one smooth and one rough side, whose size and roughness were modeled after the experimentally employed colloids with small patch size (see *SI Text* for details). We found the depletion potential to be suppressed more strongly for a depletant that is significantly smaller than the roughness inducing small hemispheres, in analogy with studies by Zhao and Mason for flat interfaces (23). While it is reasonable to expect that surface roughness will also influence depletion attractions between spherical surfaces, it has not been demonstrated previously and it is not obvious whether the difference will be significant enough to create site-selective, patchy interactions between spherical (parts of) colloidal particles.

We experimentally demonstrate site-specific attraction using nonionic dextran polymers with radii $r_p = 8.9$ nm and $r_p = 19$ nm as depletant. As shown in Fig. 1*C* significant attraction on the order of $-10\ k_BT$ between only the smooth sides of the colloids can be obtained, while attraction between rough and smooth sides and two rough sides is negligible. Optical microscopy reveals that both polymers induce specific binding between the smooth sides of the colloids. Fig. 1*E* shows timeframes of a movie in which two particles with anisotropic roughness reversibly bind and unbind at their smooth patches (Movie S1 shows the binding and unbinding event in full). Typically, single bonds last for about 10 min. Even though the rough sides of the colloids are larger than the smooth patches which for spheres implies a significantly stronger attraction, the roughness reduces the depletion potential sufficiently to suppress attraction between the larger rough sides. The alternative colloidal system with large smooth sides and small rough parts is shown in Fig. 1*D*. Clearly, depletion interactions create flexible bonds between the patches and thus allow for three-dimensional rearrangements of the bound particles.

The time required to observe such an unbinding event can be calculated using Kramers' approach (30) and taking the influence of lubrication stresses on the diffusion coefficient into account (31) (*SI Text*). The pair potential is a superposition of an Asakura-Oosawa depletion potential and a screened Coulomb potential. We employed 20 mM NaCl to decrease long-ranged electrostatic repulsions, which may reduce the effect of the roughness on the depletion potential. As a result, the minimum of the effective pair potential is significantly lowered and on the order of $-10\ k_BT$ (Fig. S5). From numerical integration we find the escape time in the case of one bond to be 630 s, in good agreement with experiments.

At higher depletant concentrations and thus stronger attractions, the roughness anisotropic colloidal particles spontaneously organize into clusters, in which the attractive parts constitute the core of the aggregate and the non-attractive rough sides are located at the outside. Representative images of colloidal clusters containing $n = 1$ to $n = 12$ particles are shown in Fig. 2*A*. Note that the colloids are free to move within the limitations of the bonds and particularly the rough parts are free to sample the accessible volume around the core of the clusters. See Fig. 2*B* for images of a cluster consisting of five dimers with various orientations of the rough sides. This flexibility in the cluster shape is due to the relatively small cone angle of the particles, which is ≈17°. For larger cone angles, simulations on cone-shaped particles found clusters with precise convex structures for $n \leq 17$ (10, 11). Additionally, in analogy with experiments on depletion driven clusters of spheres (32), for $n > 6$ the smooth sides within the core are found at various iso-energetic configurations in MC simulations and Free Energy calculations. Thus, Fig. 2*A* only shows one of the possible configuration for each cluster size.

These clusters are reminiscent of surfactant micelles, where the colloids specifically bind at their smaller smooth sides inside the clusters just like the hydrophobic parts of surfactants attract each other. The larger, rough sides of the particles are located outside of the clusters similar to the hydrophilic head group of surfactant micelles. These interactions together with their overall cone-like shape make our colloids a realization of "colloidal surfactants" (29), which in analogy to molecular surfactants form "colloidal micelles". Similar micelle-like clusters have been observed by Granick et al. for colloidal Janus-particles, whose

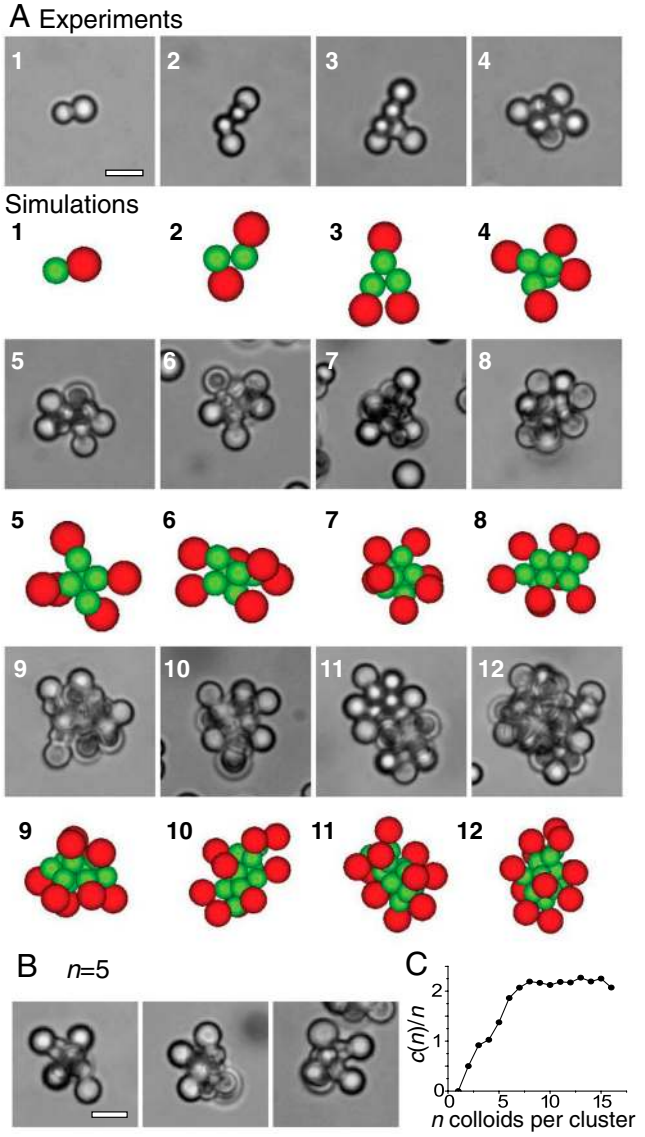

Fig. 2. *Colloidal micelles.* (*A*) Typical cluster shapes obtained from colloids with attractive small smooth, and large rough (non-attractive) side containing $n = 1$ to $n = 12$ patchy particles. Upper rows show experimentally observed clusters of colloids with small, smooth side are presented. The lower, colored rows show clusters obtained from Monte Carlo simulations on dimers consisting of a rough and a smooth sphere. The smooth spheres interact by an attractive depletion potential (green) and the rough spheres interact with a hard-sphere potential (red). The interactions between rough and smooth spheres are assumed to be hard-sphere-like. In experiments and simulations, the smaller attractive sides are located at the core of the clusters, reminiscent of micelles. Snapshots for experiments and MC simulations taken after the cluster size distribution stopped evolving significantly. (*B*) Clusters consisting of $n = 5$ colloids with a small smooth patch exhibit a variety of cluster structures because the rough parts can freely explore the available volume around the center. (*C*) Average number of bonds per particle as a function of cluster size n. Data shown is taken after 10^8 MC cycles, for $u = -9.85 k_B T$, $r_p = 19$ nm and colloids with small patch size. Scale bars are 5 μm.

surfaces are half hydrophilic and half hydrophobic (13, 14). These systems can be seen as the simplest analog of molecular surfactants, where hydrophobic and hydrophilic regions being combined in a single object cause micelle formation. Here, we present a new class of hybrid rough-smooth particles that spontaneously assemble into micelles by depletion interaction. While the origin of the driving forces for the formation of superstructures is different for the two model systems, they lead to similar, micelle-like assemblies due to their well-defined hybrid character.

The strength of the patchy attractions and thus the average number of particles in a cluster can be tuned by the polymer concentration as illustrated by Fig. 3. At low polymer concentrations $\rho_p(r_p = 19\text{ nm}) = 0.32\rho_{\text{overlap}}$, no indication of attraction between the colloidal particles is observed as illustrated in Fig. 3*A* (see Fig. S7 for experiments with polymer $r_p = 8.9$ nm in radius). Here, $\rho_{\text{overlap}} = (4\pi {r_p}^3/3)^{-1}$ is the polymer overlap concentration. An increase in the polymer concentration to $\rho_p(r_p = 19\text{ nm}) = 0.35\rho_{\text{overlap}}$ leads to small clusters, consisting mainly of two to three colloids. The binding between the particles occurs selectively at their smaller smooth sides. Based on short movies, we indicate binding between smooth sides by red arrows, and binding between a rough and a smooth side by a black/white arrow. We define the probability to observe a cluster consisting of n colloids as $P(n) = N(n)/(\Sigma_{i=1}^{n\,\max} N(i))$, where $N(n)$ is the total number of observed clusters of size n per sample. At this polymer concentration we find $P(n)$ to decrease exponentially with the colloidal cluster size which is expected if the number of bonds per cluster $c(n)$ increases linearly with n. Colloidal micelles are obtained at a slightly higher polymer concentration of $\rho_p(r_p = 19\text{ nm}) = 0.38\rho_{\text{overlap}}$. The cluster size distribution shows a significant number of single colloidal particles, equivalent to a critical micelle concentration (cmc) in surfactant systems. In this experiment the critical colloidal micelle concentration is given by the volume fraction $\Phi_{\text{exp}}^{\text{cmc}} = 3.1 \cdot 10^{-5}$. A second characteristic feature of the cluster size distribution is a peak around $n = 10$, the most probable cluster size.

The selective attraction of smooth surfaces at intermediate polymer concentrations can be demonstrated even more convincingly by the use of rough spheres with a diameter larger than the rough side of the anisotropic particles, namely 3.2 μm. The large single rough spheres, indicated by a black arrow in Figs. 1*F* and 3 are clearly excluded from the clusters despite their larger diameter, which for smooth spheres would relate to an increased depletion potential. See also Movie S2 for a rough sphere approaching a colloidal micelle without sticking, and Movie S3 for a full field view of a typical sample containing colloidal micelles.

Above a critical polymer concentration ($\rho_p(r_p = 19\text{ nm}) > 0.42\rho_{\text{overlap}}$), the site specificity of the attraction is lost. While the stronger attraction between the smooth sides still favors binding between smooth surfaces over binding between rough sides, no discrete clusters are observed, as the attractive interactions between the rough sides cannot be neglected anymore. At very high polymer concentrations ($\rho_p(r_p = 19\text{ nm}) > 0.45\rho_{\text{overlap}}$), aggregation or gel formation occurs (Fig. 3*A*).

Here, we note that the geometry of the colloids determines the cluster topology: employing colloids with smooth patches larger than the rough seed particles as shown in Fig. 1*B* leads at increasing polymer concentration first to small clusters of $n = 1$ to $n = 4$ colloids, see panel below $\rho_p(r_p = 8.9\text{ nm}) = 0.19\rho_{\text{overlap}}$ in Fig. 3*B*. Subsequently, at stronger depletion attractions induced by $\rho_p(r_p = 8.9\text{ nm}) = 0.20\rho_{\text{overlap}}$ "inverse" colloidal micelles are formed which grow without limit due to the insufficient steric protection by the rough sides. In the extreme case of smooth spheres only, growth limitations can solely be achieved by controlling the number of colloids (32). With decreasing patch size and increasing steric repulsion, or in other words a larger cone angle, we expect the cluster size distribution to shift to lower values that might even favor certain cluster sizes. (10, 11). The lower limit of the patch size is set by the physical origin of the site-specific attraction: the smooth patch size needs to be significantly larger than the scale of the roughness in order to create a sufficient difference in attraction between the patches and the rough sides. Again, above a certain polymer concentration, here $\rho_p(r_p = 8.9\text{ nm}) > 0.22\rho_{\text{overlap}}$, also the rough sides become attractive and lead to gel-like aggregates.

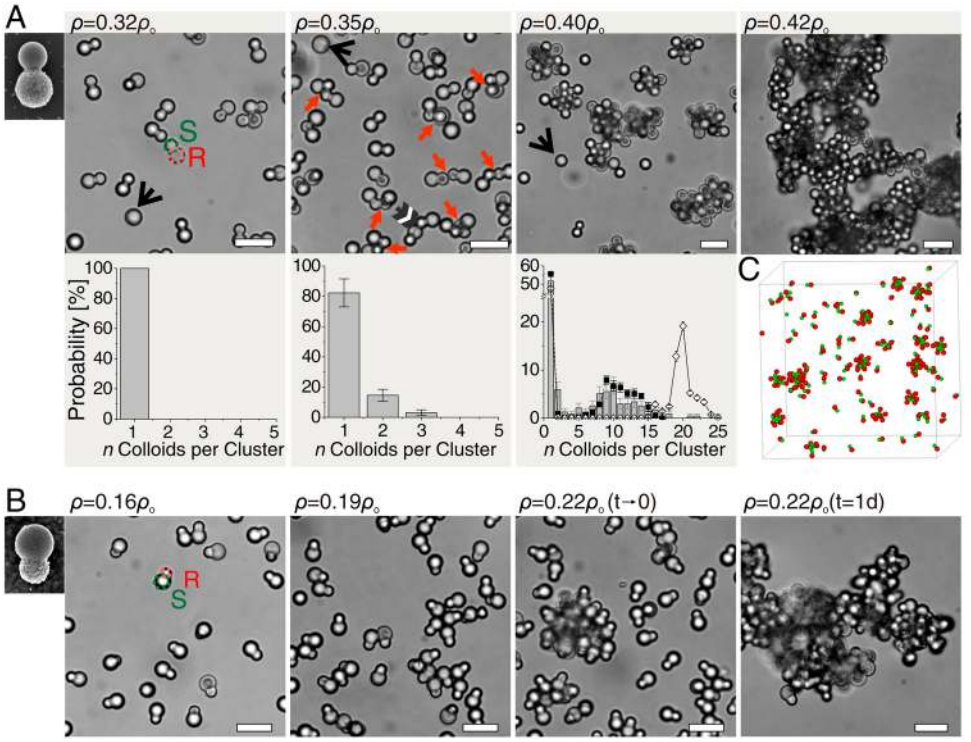

Fig. 3. *Cluster size distributions with increasing interaction strength and different geometry.* (*A*) Transmission light microscopy images of colloidal clusters from colloids with small attractive patch at increasing dextran polymer concentrations and corresponding cluster size distributions for experiments (bars, $r_p = 19$ nm), and direct MC simulations ($u = -9.85 k_B T$, $r_p = 19$ nm, after 10^8 MC cycles, filled circles) and free energy calculations (open diamond). Single particles are present in solution at $\rho_p = 0.32\rho_{overlap}$. Small clusters with an exponentially decaying size distribution for $\rho_p = 0.35\rho_{overlap}$. Bonds between smooth patches are indicated by red arrows, and black/white arrow indicates binding between smooth and rough sides of the particles. For $\rho_p = 0.40\rho_{overlap}$ a clear peak in the cluster size distribution appears around $n = 10$. Black arrows point out rough spheres. Cluster distributions shown below the microscopy images corroborate that experiments and MC simulations are in agreement. However, the distributions are not in equilibrium yet as free energy calculations yield a significantly different cluster distribution ($u = -9.85\ k_B T$ (open diamond)). Above a critical aggregation concentration site-specificity is lost. Images for $\rho_p = 0.32\rho_{overlap}$, $\rho_p = 0.35\rho_{overlap}$ and $\rho_p = 0.42\rho_{overlap}$ taken two days after sample preparation, with the first two being in equilibrium. Image for $\rho_p = 0.40\rho_{overlap}$ taken after four days, when the cluster size distribution did not evolve significantly anymore. Scale bars are 10 μm. (*B*) Transmission light microscopy images for colloids with large attractive patch at increasing attraction strength ($r_p = 8.9$ nm). Single particles are present in solution at $\rho_p = 0.16\rho_{overlap}$. Small, stable clusters form at a slightly higher polymer concentration $\rho_p = 0.19\rho_{overlap}$. Larger polymer concentrations lead to clusters that slowly grow over time: $\rho_p = 0.20\rho_{overlap}$. Above $\rho_p = 0.22\rho_{overlap}$ the rough sides become attractive as well and the site-specificity of the attraction is lost. Images taken four days after preparation. Scale bars are 10 μm. (*C*) Snapshot of a typical MC simulation showing colloidal clusters as well as free particles ($u = -9.85\ k_B T$, $r_p = 19$ nm).

We also find this sensitive dependence of the cluster size distribution on the attractive potential in direct Monte Carlo (MC) simulations in a canonical ensemble (NVT). The smooth side of the particles is modeled as a sphere of diameter σ_s interacting by an attractive Asakura-Oosawa-Vrij depletion potential (18–20) (colored in green) and the rough sides as a sphere of diameter σ_r with a hard-sphere interaction (colored in red). Interactions between the two different spheres are presumed to be hard-sphere-like. Van der Waals interactions are negligible due to electrostatic repulsions between and steric stabilization of the colloids. To take the neglected screened electrostatic repulsions into account, depletion potentials with contact values around $u = -10\ k_B T$ were employed. The simulated clusters and cluster size distributions are in excellent agreement with experiments as shown in Figs. 2 and 3*C* for $u = -9.85\ k_B T$, respectively. This implies that the observed clusters are robust with respect to the details of the interaction potentials, but sensitive to the second virial coefficient, and may be modeled by other attractive potentials as well (6). Just like in the experiments, the onset of clustering occurs abruptly with increasing bond energy. For $u = -8.9\ k_B T$ we do not find colloidal micelles, in contrast to the characteristically peaked cluster distribution shown in Fig. 3*C* for $u = -9.85\ k_B T$ The sharp transition from free monomers to colloidal micelles and larger aggregates is also consistent with the observation of gas–liquid and gas–solid transitions in colloidal spheres with short-range depletion interactions (18).

However, the cluster size distributions obtained from experiments and direct MC simulations do not agree with numerical free energy calculations on single clusters, which show strong preference for specific cluster sizes larger than those that readily formed via self-assembly, see Fig. 3 and Figs. S3 and S4 and *SI Text*. Clusters in experiments and direct MC simulations are prevented to reach full equilibrium by the short ranged, strong attractions between the patches which give rise to extremely long equilibration times. In contrast to small clusters where only one bond has to be broken to detach a colloid and thus exchange times τ of about 10 min, each particle in the colloidal micelles has to break on average 5 bonds with a bond energy $u \approx -10\ k_B T$—an event that, according to the Kramers' escape time, occurs typically every $\tau = 10^{12}$ years. Already for 2 bonds, the exchange time increases to 95 days. Sequential breaking of bonds is not likely to occur either, because particle diffusion is restricted by the remaining bonds and thus quickly leads to reformation of the bond. These long lifetimes for particles bound to more than one other particle are consistent with our experimental observations. From this we may conclude that once a particle is trapped in a micelle it will stay there indefinitely.

This irreversibility seems to be inconsistent with the observation of a background of free monomers, the cmc. However, to a

good approximation, as we will show below, the cmc depends on the average number of bonds in a cluster times the bond energy. We find that the average number of bonds first increases roughly linearly and then becomes a constant function of the average cluster size n beyond $n = 8$ (see Fig. 2*C*). Close to this cluster size, the peak in the size distribution is found as shown in Fig. 3. The strength of a bond is set by the experimental conditions (depletant, ionic strength, colloidal surface properties) and thus, the cmc becomes a constant for cluster sizes beyond around $n = 8$, irrespective of the non-equilibrium nature of the clusters. The behavior agrees with simulations on spheres interacting via a long-ranged Janus potential (2, 9).

To quantify the experimental observations we derive a formula for the critical micelle concentration considering the coexistence between single particles and clusters. The number density of unbound colloids is $\rho_1 = N(1)/V$. If ΔF is the free energy to reversibly detach a particle from the cluster, the probability to find a colloid unbound is $p(1) = N(1)/N_t = e^{-\Delta F/k_B T}$, with N_t the total number of particles. There are two contributions to the free energy ΔF: the work associated with breaking the bonds, Δu, and an entropic contribution $-T\Delta S = -k_B T \ln \Omega_0/\Omega_c$ which accounts for the difference in the number of configurations between a single particle, Ω_0 and the cluster state, Ω_c. Thus, we can write the number density of single particles as: $\rho_1 = p(1)N_t/V = N_t/V \cdot \Omega_0/\Omega_c \exp[\Delta u/k_B T]$. If we assume that detachment from a cluster liberates predominantly translational configurations, thus neglecting rotational contributions, the ratio of configurations Ω_0/Ω_c is equal to the ratio of the volumes available to the centers of mass of the particles in the two states. Assuming that monomers behave like an ideal gas, and that the fraction of free particles is small compared to the fraction of colloids in clusters, we can write $\Omega_0/\Omega_c \approx V/N_t v_{av}$, where v_{av} is the volume available for the center of mass of a particle in a cluster. Thus, $\rho_1 = v_{av}^{-1} \exp[\Delta u/k_B T]$. For our colloidal particles, this volume is equal to the volume available to the smooth spheres in a potential of range ξ. This result implies that a smaller available volume should be compensated by stronger bonds in order to maintain a constant density of single particles ρ_1, an intuitive result with an important consequence for the cluster life time, as we will show later. To illustrate the physical meaning of v_{av}, for a square well potential and a cluster consisting of $n = 2$ colloids we have $v_{av}(n = 2) = 4\pi R^2 \xi$ for $\xi \ll R$. In the limiting case of large clusters, we presume $v_{av}(n \gg 1) = \xi^3$. Then, the critical colloidal micelle concentration is given by

$$\Phi_{\text{theory}}^{\text{cmc}} = \frac{V_c}{\xi^3} e^{\Delta u/k_B T}, \qquad [1]$$

where V_c is the volume of a colloidal particle. The cmc depends on the interaction range ξ in analogy to the critical density of the phase transition between liquid and gas. We employ $\Delta u = c(n)u/(n-1)$ in analogy to the definition of the cmc in surfactant micelle systems, where $c(n)$ is the number of bonds in a cluster of size n. We take $c(n)/(n-1) = 2.4$, which is roughly the average number of bonds per particle in a cluster with energy $u = -10\ k_B T$ found in direct MC simulations. Since the cmc depends sensitively on the bond energy and the average number of bonds per particle as well as on the estimate of the interaction range, this value is expected to be accurate within an order of magnitude. We obtain $\Phi_{\text{theory}}^{\text{cmc}} = 1.3 \cdot 10^{-5}$, in good agreement with the experimentally found value of $\Phi_{\text{exp}}^{\text{cmc}} = 3.1 \cdot 10^{-5}$. Note that in case of surfactant micelles, V_c is the volume of a surfactant molecule and $v_{av} = v_s$ is the molecular volume of the solvent, which recovers the expression for the cmc of a surfactant solution (33). While the factor V_c/ξ^3 is of order unity for surfactants, for colloids the value of V_c/ξ^3 is significantly larger on the order of 10^6.

Thus, in order to have a cmc at all, i.e. $\Phi_{\text{theory}}^{\text{cmc}} < 1$, or, in more general terms, to spontaneously assemble into superstructures, significantly stronger bond energies between colloids with short-ranged interactions than between surfactant molecules are required. This implies, in turn, that according to the analysis of the escape time, equilibration times for these types of superstructures are dramatically longer. The reason for this is that the escape time of a particle is a strongly nonlinear function of the bond energy and the number of bonds of a particle in a cluster. This points to a fundamental and significant challenge in the field of equilibrium self-assembly with colloids as building blocks in situations where the difference between the available volume of the aggregated state and the dilute (monomer) state is large. This is generally the case for colloids with short-ranged interaction energies on the order of $-10\ k_B T$ per particle. In principle, it is not impossible to overcome this problem, as abundant non-equilibrium processes in biological systems show. Conceivable solutions to equilibrate colloidal systems are to apply periodic variations of the attraction strength by for example temperature sensitive depletants or single-stranded DNA, or by input of external (free) energy for instance through external fields. Equilibration problems are not expected for patchy particles with smaller patch sizes, because of fewer bonds per particles being formed.

Besides the one-patch model particles presented here, a wide variety of synthetic routes for colloids with more complex patterns of rough and smooth surfaces is readily available in literature (28, 34–40). In particular, we emphasize that size, number and even the angle between patches can be controlled (38–40). Our method to render smooth parts of colloidal particles specifically attractive can straightforwardly be applied to these particles due to its material independence and generality. To exemplify this flexibility we employ colloidal molecules with complex rough and smooth shapes, as shown in Fig. 4. Despite their different shape and patch size, they interact only at their smooth sides with other colloids. Due to the available variety of colloids and their straightforward assembly even between different patch sizes, we expect rapid advances in the controlled assembly of colloidal particles into superstructures with desired topology and properties.

The requirement of relatively strong bonds to stabilize colloidal aggregates with short-range attractions and the concomitant impact on equilibration times transcends the one-patch model system that we study. These insights are of fundamental and practical importance in the field of colloidal and macromolecular self-assembly, including proteins as building blocks. The analogy of

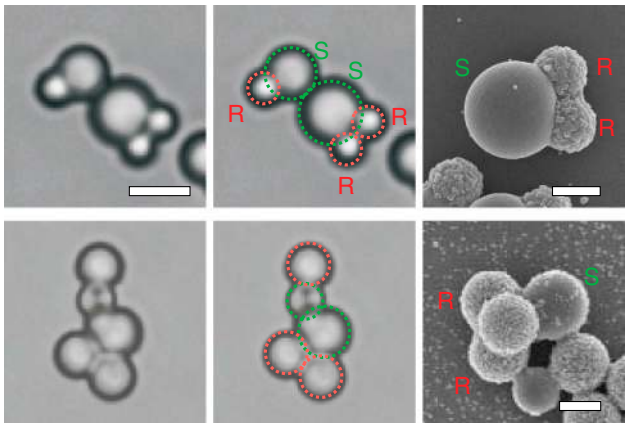

Fig. 4. *Assembly of complex rough-and-smooth colloids.* Independent of the overall complex shape, site specificity is given by the larger attraction between the smooth sides (green) than between the rough sides (red). (*A*) Colloids with two rough and one large smooth side and (*B*) with three rough and one smooth part as shown in the electron micrographs in the right panels, interact only at their smooth sides despite the larger patch size. Scale bar in left panels is 5 μm, in right panels 2 μm.

the rough-smooth colloids with molecular surfactants likely extends to emulsion and interface stabilization as well, for instance by adding spherical (and smooth) particles as a colloidal liquid phase. The model system can be straightforwardly employed to study the influence of the geometry of the colloidal surfactant on the preferred curvature of emulsion droplets, a concept often used in molecular surfactants.

Materials and Methods

Particle Synthesis. Colloidal particles consisting of one smooth and one rough sphere were synthesized following a modified synthesis by Kim et al. (27). Roughness on the seed particles was obtained through adsorption of polystyrene particles nucleated during polymerization. The synthesized colloids were washed and redispersed in 0.3% w/w aqueous polyvinyl alcohol (M_w = 30–50 kg/mol).

Sample Preparation. The samples were prepared by mixing of aqueous solution of polymer, colloidal dispersion, 20 mM NaCl, and millipore water. All components contained 7.7 mM sodium azide to prevent bacterial growth. The colloidal volume fraction was chosen to be 0.3% w/w. For depletion interaction, dextran polymers of M_w = 110 kg/mol and M_w = 500 kg/mol were dissolved in 7.7 mM aqueous sodium azide. After preparation, the samples were filled in polymer coated capillaries to prevent absorption of the particles onto the glass walls (21) and sealed with UV curable glue onto microscope slides. The microscope samples were rotated on a stage (VWR) at 10 rpm to even out effects of gravity.

Direct Monte Carlo simulations. We use Monte Carlo simulations in the canonical ensemble (*NVT*) to calculate the probability distribution of the cluster size $P(n) = N(n)/\Sigma_{i=1}^{n\,\max} N(i)$, where $N(n)$ is the number of clusters of size n in a system containing $N = 1000$ dumbbells at a packing fraction of 0.003. We consider the polymer to be of density ρ_p and diameter σ_p. The smooth side of the particles is modeled as a sphere of diameter σ_s interacting by an attractive Asakura-Oosawa-Vrij depletion potential (18–20) and the rough sides as a sphere of diameter σ_r with a hard-sphere interaction. Interactions between the two different spheres are also presumed to be hard-sphere-like. To take the neglected screened electrostatic repulsions into account, depletion potentials with contact values around $u = -10\ k_B T$ were employed. To improve mobility of clusters containing more than one particle, cluster moves are introduced which collectively move all particles that are part of the same cluster. Particles are considered to be part of the same cluster if the distance between their smooth spheres is less than the attraction range $\sigma_s + \sigma_p$.

Free Energy Calculations. The free energy of clusters of different sizes was calculated using grand-canonical Monte Carlo (GCMC) simulations on single clusters (41). We model the particles in the same way as in the direct Monte Carlo simulations, and assume that the gas of clusters is sufficiently dilute to behave as an ideal gas. To measure the cluster free energies, we simulate single clusters, and reject all moves that would break up this cluster. Apart from translation and rotation moves, we insert and remove particles according to a standard GCMC scheme. By minimizing the free energy with respect to the number of clusters of each size we find the overall cluster size distribution.

Please refer to the *SI Text* online for extended details on methods.

ACKNOWLEDGMENTS. WKK and MD thank NWO for funding via a VICI grant.

1. Zhang ZL, Glotzer SC (2004) Self-assembly of patchy particles. *Nano Lett* 4:1407–1413.
2. Sciortino F, Giacometti A, Pastore G (2010) A numerical study of one-patch colloidal particles: From square-well to janus. *Phys Chem Chem Phys* 12:11869–11877.
3. Bianchi E, Blaak R, Likos CN (2011) Patchy colloids: State of the art and perspectives. *Phys Chem Chem Phys* 13:6397–6410.
4. Bianchi E, Largo J, Tartaglia P, Zaccarelli E, Sciortino F (2006) Phase diagram of patchy colloids: Towards empty liquids. *Phys Rev Lett* 97:168301.
5. Günther Doppelbauer ea (2010) Self-assembly scenarios of patchy colloidal particles in two dimensions. *J Phys: Condens Matter* 22:104105.
6. Chen Q, Bae SC, Granick S (2011) Directed self-assembly of a colloidal kagome lattice. *Nature* 469:381–384.
7. Chen Q, et al. (2011) Supracolloidal reaction kinetics of janus spheres. *Science* 331:199–202.
8. Wilber A, Doye J, Louis A (2009) Self-assembly of monodisperse clusters: Dependence on target geometry. *J Chem Phys* 131:175101.
9. Sciortino F, Giacometti A, Pastore G (2009) Phase diagram of janus particles. *Phys Rev Lett* 103:237801.
10. Chen T, Zhang Z, Glotzer SC (2007) Simulation studies of the self-assembly of cone-shaped particles. *Langmuir* 23:6598–6605.
11. Chen T, Zhang ZL, Glotzer SC (2007) A precise packing sequence for self-assembled convex structures. *Proc Natl Acad Sci USA* 104:717–722.
12. Bianchi E, Tarlaglia P, Zaccarelli E, Sciortino F (2008) Theoretical and numerical study of the phase diagram of patchy colloids: Ordered and disordered patch arrangements. *J Chem Phys* 128:144504.
13. Hong L, Cacciuto A, Luijten E, Granick S (2006) Clusters of charged janus spheres. *Nano Lett* 6:2510–2514.
14. Hong L, Cacciuto A, Luijten E, Granick S (2008) Clusters of amphiphilic colloidal spheres. *Langmuir* 24:621–625.
15. Dendukuri D, Hatton TA, Doyle PS (2007) Synthesis and self-assembly of amphiphilic polymeric microparticles. *Langmuir* 23:4669–4674.
16. Sacanna S, Irvine WTM, Chaikin PM, Pine DJ (2010) Lock and key colloids. *Nature* 464:575–578.
17. Glotzer SC, Solomon MJ (2007) Anisotropy of building blocks and their assembly into complex structures. *Nat Mater* 6:557–562.
18. Lekkerkerker HNW, Poon WCK, Pusey PN, Stroobants A, Warren PB (1992) Phase-behavior of colloid plus polymer mixtures. *Europhys Lett* 20:559–564.
19. Asakura S, Oosawa F (1954) On interaction between two bodies immersed in a solution of macromolecules. *J Chem Phys* 22:1255–1256.
20. Vrij A (1976) Polymers at interfaces and interactions in colloidal dispersions. *Pure Appl Chem* 48:471–483.
21. Badaire S, Cottin-Bizonne C, Woody J, Yang A, Stroock A (2007) Shape selectivity in the assembly of lithographically designed colloidal particles. *J Am Chem Soc* 129:40–41.
22. Badaire S, Cottin-Bizonne C, Stroock AD (2008) Experimental investigation of selective colloidal interactions controlled by shape, surface roughness, and steric layers. *Langmuir* 24:11451–11463.
23. Zhao K, Mason T (2008) Suppressing and enhancing depletion attractions between surfaces roughened by asperities. *Phys Rev Lett* 101:148301.
24. Zhao K, Mason T (2007) Directing colloidal self-assembly through roughness-controlled depletion attractions. *Phys Rev Lett* 99:268301–.
25. Barry E, Dogic Z (2010) Entropy driven self-assembly of nonamphiphilic colloidal membranes. *Proc Nat Acad Sci* 107:10348–10353.
26. Sheu H, El-Aasser MS, Vanderhoff J (1990) Phase-separation in polystyrene latex interpenetrating polymer networks. *J Polym Sci, Part A: Polym Chem* 28:629–651.
27. Kim J, Larsen RJ, Weitz DA (2006) Synthesis of nonspherical colloidal particles with anisotropic properties. *J Am Chem Soc* 128:14374–14377.
28. Kraft DJ, et al. (2009) Self-assembly of colloids with liquid protrusions. *J Am Chem Soc* 131:1182–1186.
29. Kim J, Lee D, Shum H, Weitz D (2008) Colloid surfactants for emulsion stabilization. *Adv Mater* 20:3239–3243.
30. Kramers HA (1940) Brownian motion in a field of force and the diffusion model of chemical reactions. *Physica* 7:284–304.
31. Russel WB, Saville DA, Schowalter WA (1991) *Colloidal Dispersions* (Cambridge Univ Press, Cambridge).
32. Meng G, Arkus N, Brenner MP, Manoharan VN (2010) The free-energy landscape of clusters of attractive hard spheres. *Science* 327:560–563.
33. Israelachvili JN (1985) *Intermolecular and Surface Forces* (Academic Press Inc. Ltd., London).
34. Fujimoto K, Nakahama K, Shidara M, Kawaguchi H (1999) Preparation of unsymmetrical microspheres at the interfaces. *Langmuir* 15:4630–4635.
35. Cho Y, et al. (2005) Self-organization of bidisperse colloids in water droplets. *J Am Chem Soc* 127:15968–15975.
36. Nagao D, et al. (2010) Synthesis of hollow asymmetrical silica dumbbells with a movable inner core. *Langmuir* 26:5208–5212.
37. Yake AM, Snyder CE, Velegol D (2007) Site-specific functionalization on individual colloids: Size control, stability, and multilayers. *Langmuir* 23:9069–9075.
38. Snyder CE, Ong M, Velegol D (2009) In-solution assembly of colloidal water. *Soft Matter* 5:1263–1268.
39. Kraft DJ, Groenewold J, Kegel WK (2009) Colloidal molecules with well-controlled bond angles. *Soft Matter* 5:3823–3826.
40. Kraft DJ, et al. (2011) Patchy polymer colloids with tunable anisotropy dimensions. *J Phy Chem B* 115:7175–7181.
41. Pool R, Bolhuis PG (2005) Accurate free energies of micelle formation. *J Phys Chem B* 109:6650–6657.

Supporting Information

Kraft et al. 10.1073/pnas.1116820109

SI Text

Supporting Experimental Methods. ***Particle synthesis. Linear polystyrene spheres.*** Monodisperse linear (not cross-linked) polystyrene spheres of 1.42 μm in diameter were synthesized by dispersion polymerization. For this 126 mL ethanol (200 Proof), 14 mL deionized water, 10 mL styrene (Reagant Plus, Sigma Aldrich), 0.136 g asobisisobutyronitrile (AIBN) and 5.0 g polyvinylpyrrolidone (PVP, K30, $M_w = 40$ kg/mol) were measured into a 200 mL round bottom flask, closed with a rubber septa and sealed with Teflon tape. To commence polymerization, the flask was immersed in a 75 °C oil bath with its axis of rotation at roughly a 60° angle. Polymerization was carried out for 20 h while rotating the flask at 60 rpm.

Cross-linking of the polystyrene spheres. Typically, an aliquot of a 10% w/w linear polystyrene dispersion was washed with methanol and redispersed in 10% w/w aqueous polyvinyl alcohol (PVA, $M_w = 89$–98 kg/mol, 87–89% hydrolized) twice. After a third centrifugation step the pellet was redispersed with 1% w/w aqueous PVA such that the obtained colloidal dispersion had a weight fraction of approximately 20% w/w. For cross-linking the polystyrene particles, a procedure by Kim et al. was followed (1). A swelling emulsion consisting of 1% w/w aqueous PVA solution ($M_w = 89$–98 kg/mol) and 20% v/v styrene containing 1.5% v/v divinylbenzene, 10% v/v TMSPA (3-(trimethoxysilyl) propyl acrylate , Sigma Aldrich) and 2% w/w V65B (2,2′-azodi (2,4′-dimethylvaleronitrile), initiator)) was prepared either by tip sonication (Branson Sonifier 150, speed 8 for 2 min), or by homogenization (UltraTurrax 20, 8000 rpm for 4 min). The volume of the swelling emulsion was chosen such that a swelling ratio of 4 was achieved, where we define the swelling ratio as $S = m_{\text{monomer}}/m_{\text{polymer}}$ (2). Polymerization was carried out for 24 h while rotating in a 70 °C oil bath.

The final cross-linked particles were 2.41 ± 0.04 μm in diameter. During this step, the surface of the particles became corrugated by adsorption of polystyrene particles nucleated during polymerization, as depicted in Fig. S1*B*. The diameter of these secondary particles was roughly 0.18 μm. The dispersions of cross-linked polystyrene spheres were washed by centrifugation and redispersion in 1% w/w aqueous PVA solutions ($M_w = 89$–98 kg/mol) three times.

Protrusion formation. To obtain smooth protrusions on the cross-linked polystyrene seed particles, the previous step was repeated. A 20% w/w colloidal dispersion of cross-linked polystyrene seed particles (CPS) was swollen with an emulsion consisting of 1% w/w aqueous polyvinyl alcohol solution ($M_w = 89$–98 kg/mol) and styrene containing 1.5% v/v divinylbenzene and 2% w/w V65B. The protrusions formed by phase separation induced by an overswelling of the particles (3) have a smooth surface. They were polymerized by tumbling in an oil bath at 70 °C for 10 h. The volume of the protrusions relative to the seed particles is determined by the swelling ratio S and is continuously tunable. We note here that some batches of cross-linked seed particles produce more than one protrusion, possibly due to an inhomogeneous cross-link network. To obtain monodisperse, uniform particles we proceeded with a batch of seed particles that only yielded one protrusion per particle during this step.

For colloids with protrusions smaller than the seed particles, the seed dispersion was swollen with a 10% w/w emulsion (swelling ratio $S = 2$). The final particles have a protrusion radius of 1.11 ± 0.06 μm (smooth side, polydispersity (pd) 2.9%) and a seed radius of 1.46 ± 0.06 μm (rough side, pd 2.2%). The total length is 4.9 ± 0.12 μm (pd 2.9%). The roughness inducing secondary particles have a diameter of 185 ± 30 nm (pd 16%). A SEM image of the obtained particles is shown in Fig. S1*C*. Furthermore, large rough spheres of radius 1.6 ± 0.1 μm are employed in the experiments.

To fabricate colloids with protrusions larger than the seed particles a 20% w/w swelling emulsion with swelling ratio $S = 4$ was employed. The final anisotropic particles have a protrusion radius of 1.66 ± 0.06 μm (smooth side) and a seed radius of 1.19 ± 0.05 μm (rough side). The total particle length is 4.70 ± 0.15 μm (pd 3.2%). The roughness inducing spheres have a diameter of 182 ± 40 nm (pd 22%). A scanning electron micrograph (SEM) is shown in Fig. S1*E*.

The colloidal dispersion was washed by centrifugation until all secondary nucleated particles were removed. They were redispersed in 0.3% w/w aqueous polyvinyl alcohol solution ($M_w = 30$–50 kg/mol) to decrease the layer thickness of the steric stabilization. A schematic of the synthesis of polystyrene dimers with a rough and a smooth side is depicted in Fig. S1.

Characterization. Microscopy. Polymerized samples were imaged using a scanning electron microscope (SEM XL FEG 30, Philips). The dried samples of particles were sputter coated with 4 nm platinum/palladium prior to imaging. Light microscopy was performed with a Zeiss Axioplan microscope using an oil immersion lens (NA = 1.4, 100× magnification). Pictures were captured with a Basler scout camera and saved to disk using Streampix.

Dynamic light scattering (DLS). To measure the polymer sizes, DLS was performed with a Malvern Zetasizer ZS at a scattering angle of 173°.

Zetapotential. The surface-, or zetapotential, of the dimers was measured to be $\Psi = 0.6\ k_B T$ by laser Doppler electrophoresis with a Malvern Zetasizer ZS.

Coating of the glass capillaries. To prevent the particles from adsorbing at the glass slide in the presence of depletant, a coating was applied to the glass capillaries (4). For this, a pipette tip was connected to 50 mm borosilicate glass capillaries via elastic tubing and PTFE tape. Successively, 0.5 mL 1 M aqueous KOH (Merck), 0.5 mL millipore water, 0.5 mL 1% w/w aqueous polyethyleneimine (Fluka, $M_w = 60$ kg/mol, 50% aqueous solution), 0.5 mL millipore water, 0.5 mL 1% w/w aqueous dextran sulfate sodium salt (Acros Organics) and 0.5 mL millipore water were run through the capillaries. To remove excess polymer and salt, the capillaries were then placed in Millipore water for 10 mins and dried with nitrogen gas.

Microscope sample preparation. The samples were prepared by mixing of aqueous solution of polymer, colloidal dispersion, 20 mM NaCl (unless stated otherwise), and millipore water. All components contained 7.7 mM sodium azide (extra pure, Acros Organics) to prevent bacterial growth. The colloidal volume fraction was chosen to be 0.3% w/w. For depletion interaction, dextran polymers of $M_w = 110$ kg/mol (Fluka) and $Mw = 500$ kg/mol (Sigma Aldrich) were dissolved in 7.7 mM aqueous sodium azide (NaN_3). After preparation, the samples were filled in the capillaries and sealed with UV sensitive glue onto micro-

scope slides. To prevent sedimentation the microscope samples were rotated at 10 rpm (VWR stage).

Supplementary Computational Methods. ***Effective pair potentials between colloidal spheres with rough or smooth surfaces.*** The colloidal particles with a rough surface are modeled as hard spheres with diameter σ_r at positions $\mathbf{R}_i$ coated with small hard spheres on the colloidal surface. We consider N_c coated particles with orientations $\hat{\omega}_i$ and N_p polymers with diameter σ_p at positions $\mathbf{r}_j$ in a macroscopic volume V at temperature T. The polymer diameter $\sigma_p = 2r_p$ is taken to be twice the radius of gyration r_p. The colloidal particles are described by a pairwise colloid-colloid interaction Hamiltonian $H_{cc} = \Sigma_{i<j}^{N_c}\phi_{cc}(\mathbf{R}_{ij}, \hat{\omega}_i, \hat{\omega}_j)$, a pairwise colloid-polymer Hamiltonian $H_{cp} = \Sigma_{i=1}^{N_c}\Sigma_{j=1}^{N_p}\phi_{cp}(\mathbf{R}_i - \mathbf{r}_j, \hat{\omega}_i)$, and a polymer-polymer Hamiltonian $H_{pp} \equiv 0$ as the polymers are assumed to be ideal. Here we introduced the colloid-colloid pair potential ϕ_{cc} and the colloid-polymer pair potential ϕ_{cp} given by

$$\beta\phi_{cc}(\mathbf{R}_{ij}, \hat{\omega}_i, \hat{\omega}_j) = \begin{cases} \infty & \text{for } \xi(\mathbf{R}_{ij}, \hat{\omega}_i, \hat{\omega}_j) < 0 \\ 0 & \text{otherwise} \end{cases}$$

$$\beta\phi_{cp}(\mathbf{R}_i - \mathbf{r}_j, \hat{\omega}_i) = \begin{cases} \infty & \text{for } \xi(\mathbf{R}_i - \mathbf{r}_j, \hat{\omega}_i) < 0 \\ 0 & \text{otherwise} \end{cases},$$

where $\beta = (k_B T)^{-1}$ with k_B the Boltzmann constant, and where $\mathbf{R}_{ij} = \mathbf{R}_i - \mathbf{R}_j$, $\xi(\mathbf{R}_{ij}, \hat{\omega}_i, \hat{\omega}_j)$ denotes the surface-to-surface distance between two coated particles, and $\xi(\mathbf{R}_i - \mathbf{r}_j, \hat{\omega}_i)$ is the surface-to-surface distance between a coated particle and a polymer coil. The total interaction Hamiltonian of the system of interest reads $H = H_{cc} + H_{cp}$. The kinetic energy of the polymers and the colloids is not considered here explicitly, as it is trivially accounted for in the classical partition sums to be evaluated below.

We map the binary mixture of coated particles and ideal polymers with interaction Hamiltonian H onto an effective one-component system with Hamiltonian H^{eff} by integrating out the degrees of freedom of the polymer coils. Our derivation follows closely that of ref. (5).

We consider the system in the (N_c, V, z_p, T) ensemble, in which the fugacity $z_p = \Lambda_p^{-3}\exp(\beta\mu_p)$ of the polymer coils is fixed, with Λ_ν the thermal wavelength of species $\nu = c, p$, and with μ_p the chemical potential of the polymers. The thermodynamic potential $F(N_c, V, z_p, T)$ of this ensemble can be written as

$$\begin{aligned}\exp[-\beta F] &= \sum_{N_p=0}^{\infty}\frac{z_p^{N_p}}{N_c!\Lambda_c^{3N_c}N_p!}\,\text{Tr}_c\,\text{Tr}_p\exp[-\beta H] \\ &= \frac{1}{N_c!\Lambda_c^{3N_c}}\,\text{Tr}_c\exp[-\beta H^{\text{eff}}], \qquad \text{[S1]}\end{aligned}$$

where the trace Tr_c is short for the volume integral $\int_V d\mathbf{R}^{N_c}$ $\int_\Omega d\hat{\omega}^{N_c}$ over the coordinates and orientations of the coated particles, and similarly $\text{Tr}_p = \int_V d\mathbf{r}^{N_p}$. The effective Hamiltonian of the coated particles can be written as

$$H^{\text{eff}} = H_{cc} - z_p V_f, \qquad \text{[S2]}$$

where $z_p V_f = z_p V_f(\{\mathbf{R}\}, \{\hat{\omega}\})$ is the negative of the grand potential of the fluid of ideal polymer coils in the static configuration of N_c coated colloids with coordinates $\{\mathbf{R}\}$ and orientations $\{\hat{\omega}\}$. Here $V_f(\{\mathbf{R}\}, \{\hat{\omega}\})$ is the free volume of the polymers in the configuration of the colloids. Because of the ideal character of the polymer-polymer interactions it can be written explicitly as

$$V_f = \int_V d\mathbf{r}\exp\Big[-\sum_{i=1}^{N_c}\beta\phi_{cp}(\mathbf{R}_i - \mathbf{r}, \hat{\omega}_i)\Big]. \qquad \text{[S3]}$$

Non-vanishing contributions to V_f stem from those positions $\mathbf{r}$ that are outside any of the N_c depletion shells. The shape of the free volume is highly irregular and non-connected. We decompose V_f, formally, into zero-colloid, one-colloid, two-colloid contributions, etc., by expanding it in terms of the colloid-polymer Mayer-function $f(\mathbf{R}_i - \mathbf{r}, \hat{\omega})$, which for the present model equals -1 for $\xi(\mathbf{R}_i - \mathbf{r}, \hat{\omega}) < 0$, and 0 otherwise. One finds

$$\begin{aligned}V_f &= \int_V d\mathbf{r}\prod_{i=1}^{N_c}(1 + f(\mathbf{R}_i - \mathbf{r}, \hat{\omega})) \\ &= V + \sum_{i=1}^{N_c}V_f^{(1)}(\mathbf{R}_i, \hat{\omega}_i) + \sum_{i<j}^{N_c}V_f^{(2)}(\mathbf{R}_i, \mathbf{R}_j, \hat{\omega}_i, \hat{\omega}_j) + \cdots \qquad \text{[S4]}\end{aligned}$$

For $k \geq 1$, the k-colloid contribution reads

$$V_f^{(k)} = \int_V d\mathbf{r}\prod_{m=1}^{k}f(\mathbf{R}_{i_m} - \mathbf{r}, \hat{\omega}_{i_m}), \qquad \text{[S5]}$$

where only those positions $\mathbf{r}$ give non-vanishing contributions where the depletion layers of (at least) k colloids overlap simultaneously.

We give explicit expressions for $V_f^{(k)}$ for $k = 1$ and 2 for equal-sized colloidal hard spheres with a smooth surface. It follows directly from Eq. **S4** that the one-body contribution $V_f^{(1)} = -v_1$ with $v_1 = \pi\sigma_{cp}^3/6$ and $\sigma_{cp} = (\sigma_r + \sigma_p)/2$, which can be interpreted as the volume that is excluded for a polymer coil by a single colloid. $V_f^{(2)}(\mathbf{R}_i, \mathbf{R}_j)$ is the lens-shaped overlap volume as depicted in Fig. 1*B* of two spheres of radius σ_{cp} at separation $R_{ij} = |\mathbf{R}_i - \mathbf{R}_j|$. We note that $-z_p V_f^{(2)}(R_{ij}) \equiv \beta\phi_{\text{AO}}(R_{ij})$ is the well-known depletion potential of the AO model (6, 7), which was derived by Asakura and Oosawa as well as Vrij (8, 9). The effective pair potential $\phi_{\text{eff}}(R_{ij}) = \phi_{\text{cc}}(R_{ij}) + \phi_{\text{AO}}(R_{ij})$ reads

$$\beta\phi(R_{ij}) = \begin{cases} \infty & \text{for } R_{ij} < \sigma_r \\ -\frac{\pi\sigma_p^3 z_p}{6}\frac{(1+q)^3}{q^3}\left[1 - \frac{3R_{ij}}{2(1+q)\sigma_r} + \frac{R_{ij}^3}{2(1+q)^3\sigma_r^3}\right] & \text{for } \sigma_r < R_{ij} < \sigma_r + \sigma_p \\ 0 & \text{for } R_{ij} > \sigma_r + \sigma_p \end{cases}.$$

This Asakura-Oosawa pair potential describes an attractive well close to the surface of the colloid, whose depth increases linearly with increasing z_p. The range of the potential is given by σ_p.

Similarly, we define an effective depletion potential for our coated spheres, which depends explicitly on the orientation of the coated spheres.

$$\begin{aligned}\beta\phi_{\text{eff}}(\mathbf{R}_{ij}, \hat{\omega}_i, \hat{\omega}_j) &= \beta\phi_{\text{cc}}(\mathbf{R}_{ij}, \hat{\omega}_i, \hat{\omega}_j) \\ &\quad - z_p\int_V d\mathbf{r} f(\mathbf{R}_i - \mathbf{r}, \hat{\omega}_i)f(\mathbf{R}_j - \mathbf{r}, \hat{\omega}_j). \qquad \text{[S6]}\end{aligned}$$

The three- and more-body contributions $V_f^{(k)}$ with $k \leq 3$ will be zero when the radius of gyration of the polymer coils is sufficiently small compared to the size of the colloids. The mapping of the full Hamiltonian of the colloid-polymer mixture can then be mapped exactly onto an effective Hamiltonian with only

effective pairwise additive interactions, since three colloidal spheres cannot simultaneously overlap with a polymer coil. If the relaxation of the orientation degrees of freedom is much faster than that of the translational degrees of freedom, and the coated particles are sufficiently isotropic, we can perform a further coarse-graining by integrating out the orientational degrees of freedom of the effective interactions. The orientation-averaged effective pair potential reads

$$\beta\phi_{\text{eff}}(R_{ij}) = -\log\left(\frac{1}{16\pi^2}\int_\Omega d\hat{\omega}_i \int_\Omega d\hat{\omega}_j \exp\left[-\beta\phi_{\text{cc}}(\mathbf{R}_{ij},\hat{\omega}_i,\hat{\omega}_j) - z_p\int_V d\mathbf{r} f(\mathbf{R}_i-\mathbf{r},\hat{\omega}_i) f(\mathbf{R}_j-\mathbf{r},\hat{\omega}_j)\right]\right). \quad \text{[S7]}$$

Since the integrals over the orientations of the particles cannot be solved directly, we perform the orientation average by evaluating the integrand for many different random orientations. We have checked the convergence of our integrations.

In order to generate colloidal particles coated with small particles onto the surface, we perform Monte Carlo simulations of a binary mixture of oppositely charged particles in the NVT ensemble. The particles are assumed to interact with Yukawa interactions and we choose a negative charge on the small particles and a positive charge on the large particles. The charge magnitude was increased until all the small particles were attached onto the surface of the large particles. The structure of the small particles on the surface of the large particles can be tuned by the inverse screening length $\kappa\sigma_r$ in the Yukawa interaction of the particles. For low $\kappa\sigma_r$ the small particles are evenly distributed and very structured while for high $\kappa\sigma_r$ there is much more disorder in the coating of the small spheres. Using $\kappa\sigma_r = 10$, the resulting configurations gave the best match with the coated particles as employed in the experiments and as shown in Fig. 1*A*.

Once the two particles have been created they are placed next to each other in a cubic simulation box and 1×10^5 random orientations of the two particles are sampled. For the first 1000 non-overlapping configurations, we determine the effective pair potential. If non-overlapping configurations were found the particles are moved closer together and again orientations are generated and the potential calculated. To calculate the free volume we divide the space into cells. To calculate the overlap volume in each cell we first check whether the cell is completely embedded in the overlap volume or falls completely outside the overlap volume. If neither is the case the cell is divided into eight subcells for which we perform the same procedure. This is repeated until the volume of the cell is smaller than $1\times10^{-5}\sigma_r^3$, the algorithm then randomly generates ten points to estimate the overlap volume in this cell. The final overlap volume is than the sum of the overlap volumes of all cells. We tested the accuracy of this method for two spheres and the difference between the analytic expression and the calculation is less than $1\times10^{-5}\sigma_r^3$.

We calculated the effective pair potential for two rough spheres including the rough surface layer and the effective pair potential for a rough and a smooth sphere. The smooth spheres in this system have a diameter of $\sigma_s = 2.22$ μm, the rough spheres have a diameter of $\sigma_r = 2.92$ μm including the rough surface layer, the small spheres that form the roughness have a diameter of 185 nm and the polymers have diameters of 38 nm. In Fig. 1*C* we plot the effective pair potential between two smooth spheres, two rough spheres and one rough and one smooth sphere for a polymer reservoir density $\rho_p^r = 0.038\ \rho_{\text{overlap}}$. We find significant attraction between the smooth spheres, while the attraction between a rough and a smooth sphere and between two rough spheres is negligible.

Direct simulations. We model the system as N asymmetric dumbbells consisting of a rough sphere and a smooth sphere in volume V with ideal polymer of density ρ_p and diameter σ_p. The diameters of the rough and smooth spheres are $\sigma_r = 2.92$ μm and $\sigma_s = 2.22$ μm, respectively. The effective pair potential for two smooth spheres is given by the Asakura-Oosawa depletion potential (6), where σ_r is replaced by σ_s and $q = \sigma_p/\sigma_s$ is the size ratio between the polymer and smooth spheres. The rough spheres are treated as hard spheres and the effective pair potential between rough and smooth spheres are assumed to be hard-sphere-like. We use Monte Carlo simulations in the canonical ensemble (NVT) to calculate the probability distribution of the cluster size $P(n) = N(n)/\Sigma_{n=1}^{n_{\max}} N(n)$, where $N(n)$ is the number of clusters of size n in a system containing $N = 1000$ dumbbells at a packing fraction of 0.003. To improve mobility of clusters containing more than one particle, cluster moves are introduced which collectively move all particles that are part of the same cluster. Particles are considered to be part of the same cluster if the distance between their smooth spheres is less than the attraction range $\sigma_s + \sigma_p$. Fig. S2 shows typical configurations of the MC simulations for two polymer sizes, $\sigma_p = 38$ and 16 nm. We clearly observe the formation of micelle-like clusters in addition to single dumbbell particles. The cluster size distributions are shown along with the experimental one in Fig. 3*C* for $\sigma_p = 38$ nm and in Fig. S6 for $\sigma_p = 16$ nm. Finally, we present typical configurations of the clusters containing $n = 1$ to $n = 15$ particles in Fig. 2 together with the experimental images.

Free energy calculations. The free energy of clusters of different sizes can be calculated using grand-canonical Monte Carlo (GCMC) simulations on single clusters. A similar method has previously been used to study the formation of micelles from surfactants (10). We model the particles in the same way as in the direct Monte Carlo simulations, and assume that the gas of clusters is sufficiently dilute to behave as an ideal gas. The partition function for the total system of clusters is then given by:

$$Q = \prod_{n=1}^{\infty}\frac{Q_n^{N_n}}{N_n!}, \quad \text{[S8]}$$

$$Q_n = \frac{1}{(4\pi)^n\Lambda^{3n}n!}\int_V d\mathbf{r}^n\int d\mathbf{n}^n \exp(-\beta U(\mathbf{r}^n,\mathbf{n}^n))h(\mathbf{r}^n,\mathbf{n}^n), \quad \text{[S9]}$$

where N_n is the number of clusters of size n, Λ is the coarse-grained length scale (e.g. in atomic systems the De Broglie wavelength), $\beta = 1/k_{\text{B}}T$, and $\mathbf{r}^n$ and $\mathbf{n}^n$ denote the positions and orientations of the dumbbell particles, respectively. The function $h(\mathbf{r}^n,\mathbf{n}^n)$ equals 1 if the particles with centers $\mathbf{r}^n$ and orientations $\mathbf{n}^n$ form a single cluster, and 0 otherwise. For an ideal gas of these particles, with only clusters of size 1, this yields the ideal gas free energy $\beta F/N = \log\rho\Lambda^3 - 1$. The partition function can also be written as:

$$Q = \prod_{n=1}^{\infty}\frac{(V/\Lambda^3)^{N_n}}{N_n!}\left(\frac{Q_n}{Q_1}\right)^{N_n}. \quad \text{[S10]}$$

Here, Q_n/Q_1 is the ratio of the partition function of a cluster of n particles to that of a cluster of one particle. This ratio can be measured from a grand-canonical Monte Carlo simulation, at fixed chemical potential μ. In a GCMC with the additional constraint that all particles should form a single cluster, the probability $P(n)$ of observing a cluster of size n obeys:

$$\frac{P(n)}{P(1)} = \exp[\beta\mu(n-1)]\frac{Q_n}{Q_1}. \quad \text{[S11]}$$

Hence, the ratios Q_n/Q_1 can be directly obtained from the GCMC simulations. These ratios are independent of μ, although simulations at different values of μ can be employed to sample all cluster sizes.

To find the cluster distribution of a system with an overall particle density ρ, we simply minimize the free energy $F = -k_B T \log Q$ with respect to the number of clusters of each size. This yields:

$$\rho_n \Lambda^3 = (\rho_1 \Lambda^3)^n \exp(-\beta(f_n - f_1)), \qquad \textbf{[S12]}$$

with $f_n = -k_B T \log(Q_n)$ the free energy of a cluster of size n. From this, it is straightforward to calculate the cluster size distribution for any overall system density. Note that the choice of Λ does not influence the results.

To measure the cluster free energies f_n, we simulate single clusters, and reject all moves that would break up this cluster. Apart from translation and rotation moves, we insert and remove particles according to a standard GCMC scheme, again restricting the system to single clusters. The box volume has no influence on the outcome of the simulation, as insertions will only be accepted near the cluster. In fact, only insertions inside the attractive wells of existing particles can be accepted without resulting in two separate clusters, so only insertion moves inside those wells are attempted. The volume in the normal acceptance rule for a GCMC insertion move is then replaced by the volume of n spherical shells with the size of the attractive well, where n is the number of particles in the system. As the potential wells of multiple particles can overlap, a correction is required to satisfy detailed balance when a particle is inserted into the attractive well of more than one neighboring particles. After normal acceptance, the move is only accepted with a probability of $1/k$, where k is the number of overlapping wells at the point of insertion.

To calculate the cluster size distributions, the free energy of a range of cluster sizes is needed. As the resulting cluster size can be very sensitive to the chemical potential, it is more convenient to set $\mu = 0$, and to implement a standard Umbrella Sampling scheme to sample the required cluster sizes instead. To improve sampling speed at high interaction strengths, we use parallel tempering. Each simulation contains a number of separate clusters, each at a different interaction strength, but biased towards the same cluster size. While the different clusters do not interact, a new Monte Carlo move is introduced that swaps configurations of two different interaction strengths.

If the interactions are weak, the distributions obtained from free energy calculations closely match those from the direct simulations. However, when the interactions are strong enough that larger clusters are formed, the equilibrium distributions show a strong preference for specific cluster sizes much larger than those seen in the direct simulations (see Fig. S3). Clusters around size 10 are not found in significant quantities for any interaction strength. In particular, at the packing fraction and interaction range used in the experiments and the direct simulations, cluster sizes 19, 20, 22, and 23 all appear as common cluster sizes, depending on the polymer concentration. Figures of typical clusters of these sizes are shown in Fig. S4. These clusters all display a large number of bonds per particle, and the smooth spheres in the micelles show crystalline order, with a tetrahedral structure (marked in pink) at the center. Forming these clusters spontaneously would require a large number of reorganizations including breaking several bonds. As explained earlier, this will not happen within a reasonable time scale.

It is interesting to note that the cluster sizes preferred in these distributions do not always maximize the number of bonds per particle, which would minimize the potential energy of the cluster. For example, from the clusters of sizes 19, 20, 22, and 23 shown in Fig. S4, the lowest-energy cluster is size 22, with 6.545 bonds per particle, but this size is not particularly common in the distributions in Fig. S3. Clearly, entropic effects still need to be taken into account to predict what clusters will appear more often.

Supplementary Derivations. ***Interaction potential.*** The short ranged depletion attraction between the colloids is significantly lowered by the screened Coulomb repulsions. We take the attractive depletion potential to be Eq. **S6** and the screened Coulomb potential to be:(11)

$$u_{el}(x) = \frac{\Psi^2 (\sigma_s/2)^2}{\lambda_B x} \exp[-\kappa(x - \sigma_s)], \qquad \textbf{[S13]}$$

where σ_s is the diameter of the smooth side of the colloids, $\Psi = 0.6\ k_B T$ is the zetapotential of the particles measured by laser doppler electrophoresis, $\lambda_B = 0.71$ nm is the Bjerrum length in water, and κ is the inverse of the Debye screening length, and x is the distance between the centers of the two particles. At 20 mM NaCl, $\kappa \approx 0.5\ \text{nm}^{-1}$. The Asakura-Oosawa potential (AO) is plotted together with the screened Coulomb repulsion (C) in Fig. S5. For polymer concentrations at which clustering was observed, the minimum of the total potential (tot) is roughly $-5\ k_B T$ for the polymer with 8 nm radius (Fig. S5*A*), and $-17\ k_B T$ for polymer with 19 nm radius (Fig. S5*B*). Clearly, screened Coulomb repulsion significantly reduces the short-ranged depletion potential. However, the actual value for the interaction strength may be different as the minimum of the potential energy strongly depends on value of the zetapotential, namely as $u_{el} \propto \Psi^2$. The error associated with measuring the zetapotential on anisotropic particles thus makes the values obtained from screened Coulomb potentials approximative.

Escape rate for a single particle from a cluster. A particle diffusing in an energy potential well $u(x)$ with x the distance to closest approach and minimum at position b can escape that well with rate $r = \tau^{-1}$. We numerically calculate the escape time τ using Kramer's approach (12):

$$\tau = \int_a^c e^{-u(x)/k_B T} dx \int_b^e \frac{1}{D(y)} e^{u(y)/k_B T} dy. \qquad \textbf{[S14]}$$

Because the interaction range and thus the separation between interacting particles is short compared to the particle diameter, the problem is essentially one-dimensional. Here, $D(y)$ is the effective colloid diffusion constant in the well, which depends on the separation y between the colloids due to lubrication effects as: (13)

$$D(y) = \frac{8y}{\sigma_s} D_0, \qquad \textbf{[S15]}$$

D_0 is the diffusion constant for an unperturbed particle and can be calculated from the Einstein relation. Given the parameters in our system, where we estimated the viscosity to be $\eta = 2$ mPa·s (14), the diffusion constant D_0 is roughly $1 \cdot 10^{-13}\ \text{m}^2/\text{s}$.

We integrated the total potential as shown in Fig. S5 numerically for different numbers of bonds. To compare the results with the experimental values for the escape times, we scale the energy axis such that the minimum for one bond corresponds to $-10\ k_B T$ as was deduced from the simulations. We chose the values for the integration boundaries as follows: $a = 5$ nm and $c = 20$ nm. The precise values of a and c are arbitrary but irrelevant. The minimum b is located at 10 nm, where again the precise value is not critical. However, the result depends fairly strongly on the choice of the upper integration limit e, see Eq. **S14**, which is the point were we consider the particle to have escaped from the dimer. Experimentally the particle must have traveled a few hundred nanometers before the observer decides whether the particle has escaped. Therefore, a natural choice for this boundary is a

few hundred nanometers. Here we took $e = 400$ nm. With this input the escape time from a dimer is found to be 630 s. This result seems consistent with direct observations from light microscopy, where typically 10 min is observed for a particle to escape from a dimer. For comparison, the theoretical time to reach a hypothetical escape at $d = 38$ nm, which is the range of the potential, is 54 s. For the observer, the particle has not escaped yet, even if it is outside the influence of the potential, because it still has a large chance to diffuse back into the trap without the observer noticing it had 'escaped'.

If we calculate the escape time to break two bonds with the escape distance being located at 400 nm we find 95 days. To break three bonds it takes 4000 years according to these calculations and to break five bonds about $1 \cdot 10^{12}$ years. These long lifetimes for more than one bond are consistent with the fact that we have not observed such events in our experiments.

Supplementary experiments. Besides the experiments with dextran polymer of $r_p = 19$ nm as depletant, we also employed a smaller sized dextran polymer $r_p = 8.9$ nm in size. Fig. S6 shows transmission light micrographs of samples at increasing polymer concentration. At a polymer concentration of $\rho_p = 0.16\rho_{\text{overlap}}$, the depletion potential is insufficient to cause aggregation between the colloidal particles. A slightly higher polymer concentration of $\rho_p = 0.19\rho_{\text{overlap}}$ induces attractions between the smooth, small sides of the colloidal particles, leading to small clusters of $n = 1$ to $n = 4$ colloids in size. Above polymer concentrations of $\rho_p = 0.22\rho_{\text{overlap}}$ formation of colloidal clusters with the attractive and smooth sides of the dumbbells at the inside occurs. All data shown was taken after 9 days. The distributions for $\rho_p = 0.16\rho_{\text{overlap}}$ and $\rho_p = 0.19\rho_{\text{overlap}}$ did not evolve anymore after 1 day, the distribution for $\rho_p = 0.22\rho_{\text{overlap}}$ did not evolve significantly anymore after a few days. Qualitatively this aggregation behavior is comparable to the observations on the larger depletant as shown in Fig. 3 of the manuscript. Quantitatively, there are differences in the agreement of the cluster size distributions of the experiments and simulations as shown in Fig. S6. Clearly, only a weak agreement is obtained, with experiments showing a wide range of clusters sizes in contrast to the peak found in simulations. The range of the depletion potential is roughly the diameter of the depletant, and thus, for the smaller polymer shorter by more than a factor 2 compared to the larger polymer. Within these short-ranged attractive potentials rearrangement of the clusters is difficult and equilibration experimentally not achievable within a reasonable time-scale. Estimates of the added screened Coulomb-interaction and depletion interactions also indicate a deeper minimum compared to the larger polymer. The shorter interaction range and the stronger maximum attraction are likely the cause for the increased equilibration times.

1. Kim J-W, Larsen R, Weitz DA (2006) Synthesis of nonspherical colloidal particles with anisotropic properties. *J Am Chem Soc* 128:14374–14377.
2. Sheu H, El-Aasser MS, Vanderhoff J (1990) Phase-separation in polystyrene latex interpenetrating polymer networks. *J Polym Sci Part A: Polym Chem* 28:629–651.
3. Kegel WK, Breed D, Elsesser M, Pine DJ (2006) Formation of anisotropic polymer colloids by disparate relaxation times. *Langmuir* 22:7135–7136.
4. Badaire S, Cottin-Bizonne C, Woody J, Yang A, Stroock A (2007) Shape selectivity in the assembly of lithographically designed colloidal particles. *J Am Chem Soc* 129:40–41.
5. Dijkstra M, Brader JM, Evans R (1999) Phase behaviour and structure of model colloid-polymer mixtures. *J Phys: Condens Matt* 11:10079–10106.
6. Vrij A (1976) Polymers at interfaces and the interactions in colloidal dispersions. *Pure Appl Chem* 48:471–483.
7. Gast AP, Hall CK, Russel WB (1983) Polymer-induced phase separations in nonaqueous colloidal suspensions. *J Colloid Interface Sci* 96:251–267.
8. Asakura S, Oosawa F (1954) On interaction between two bodies immersed in a solution of macromolecules. *J Chem Phys* 22:1255–1256.
9. Asakura S, Oosawa F (1958) Interaction between particles suspended in solutions of macromolecules. *J Polym Sci* 33:183–192.
10. Pool R, Bolhuis PG (2005) Acurate free energies of micelle formation. *J Phys Chem B* 109:6650–6657.
11. Verwey EJW, Overbeek JThG (1948) *Theory of the Stability of Lyophobic Colloids* (Elsevier, New York).
12. Kramers HA (1940) Brownian motion in a field of force and the diffusion model of chemical reactions. *Physica* 7:284–304.
13. Russel WB, Saville DA, Schowalter WA (1991) *Colloidal Dispersions*, (Cambridge Univ Press, Cambridge, UK), Chapter 2.8.
14. Gündüz U (1996) Evaluation of viscosities of polymer-water solutions used in aqueous two-phase systems. *J Chromatogr B: Anal Technol Biomed Life Sci* 6880:263–266.

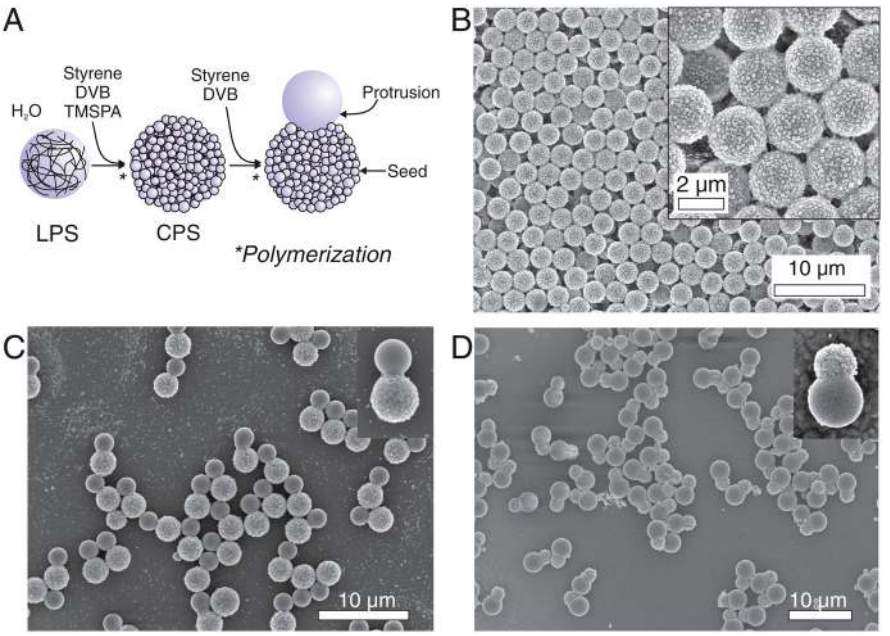

Fig. S1. Schematic synthesis of patchy particles. (*A*) Linear polystyrene (LPS) spheres are crosslinked by swelling with an emulsion consisting of styrene, divinylbenzene (DVB), and 3-(trimethoxysilyl)propyl acrylate (TMSPA). During polymerization, secondary nucleated particles render the particle surface rough by adsorption. SEM image of the rough spheres is shown in *B*. A second swelling step with an emulsion consisting of styrene and DVB yields rough particles with a smooth protrusion, as shown in *C*. (*D*) Transmission light micrograph of the particles in *C*. (*E*) SEM image of particles with smooth protrusions larger than the rough seed particles.

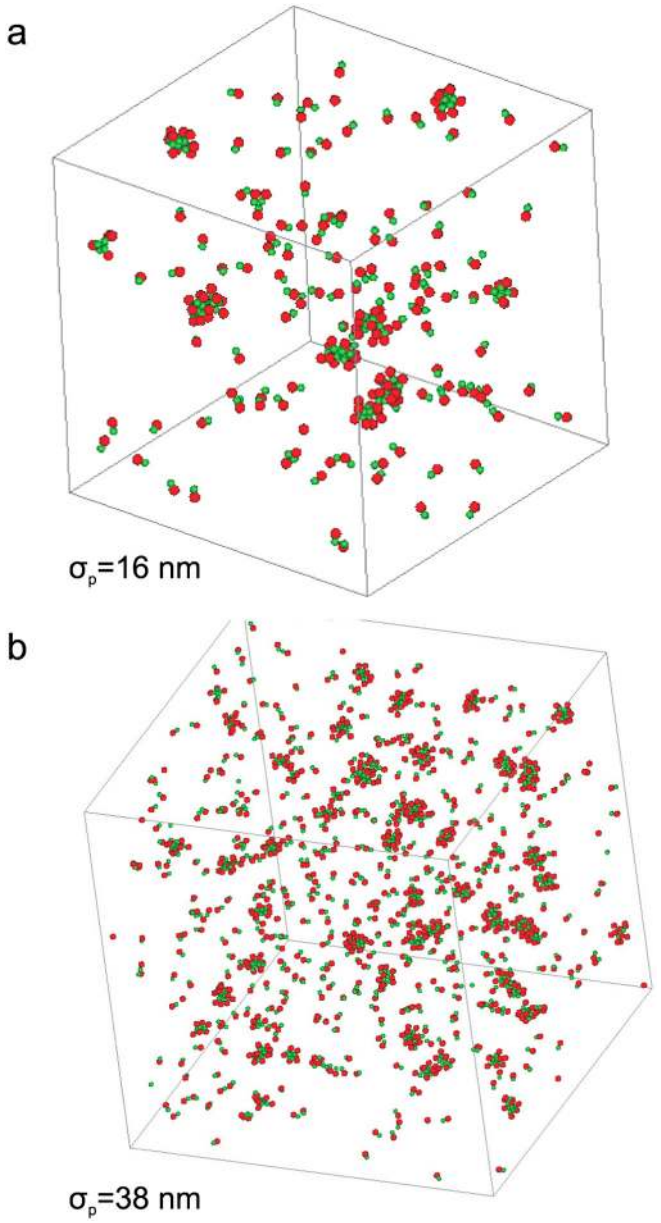

Fig. S2. Snapshots of Monte Carlo simulations after 10^8 MC cycles performed on dimers with one attractive sphere (green) and one hard sphere (red) modeled after the experimentally employed colloids. An attractive Asakura-Oosawa-Vrij potential between the green spheres of the dimers is induced by the addition of polymers with a diameter (*A*) $\sigma_p = 16$ nm, and (*B*) $\sigma_p = 38$ nm. Micelle-like clusters are visible next to single colloids.

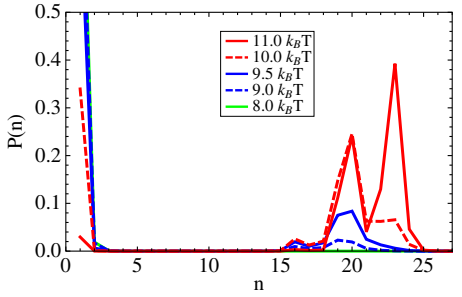

Fig. S3. Equilibrium cluster size distributions of dumbbells consisting of a rough and a smooth sphere with size ratio $\sigma_s/\sigma_r = 0.76$ at various interaction strengths (contact value ranging from 8 to 11 $k_B T$), using the experimental packing fraction $\eta = 0.003$ and polymer size $\sigma_p/\sigma_s = 0.02$.

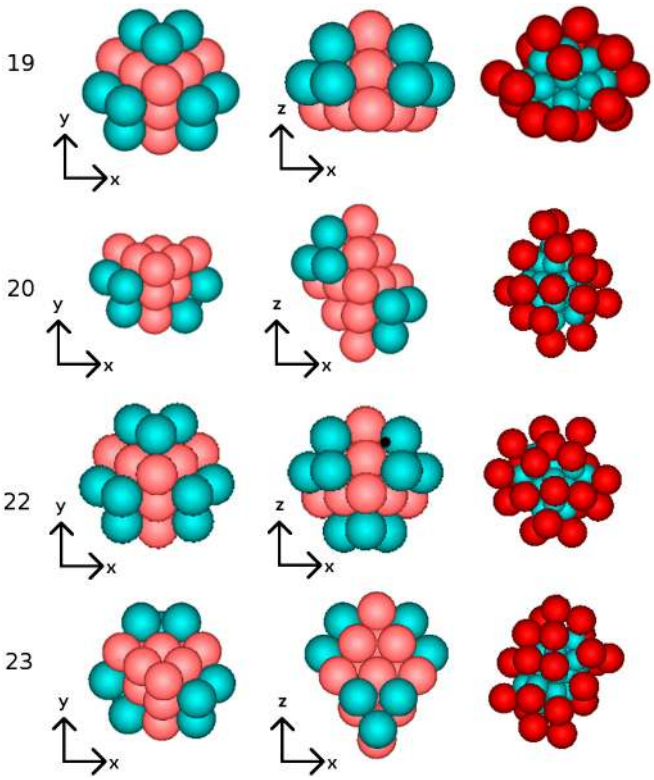

Fig. S4. Typical clusters of common sizes in the equilibrium distributions. For each size, two snapshots are shown where the rough spheres are removed, and one with the rough spheres included.

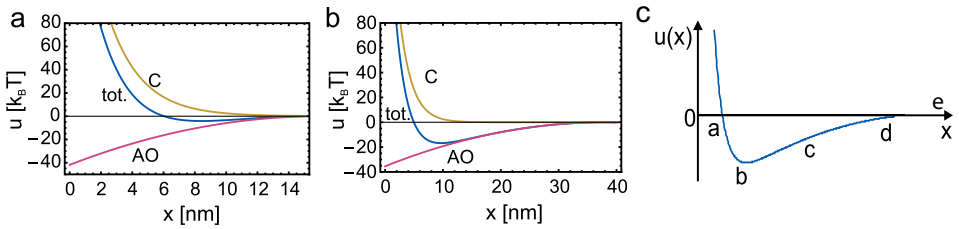

Fig. S5. A short-ranged screened Coulomb repulsion (C) reduces the Asakura-Oosawa (AO) depletion potential considerably, yielding an overall potential (tot) with a much smaller absolute minimum energy. Potential energies are plotted as a function of the distance x between surfaces of the two spheres. (*A*) Shows the potentials for $r_p = 8.9$ nm and $\rho_p = 0.2\rho_{\text{overlap}}$, and (*B*) for $r_p = 19$ nm and $\rho_p = 0.4\rho_{\text{overlap}}$. (*C*) Schematic interaction potential to illustrate the integration boundaries used to calculate the Kramer's escape time.

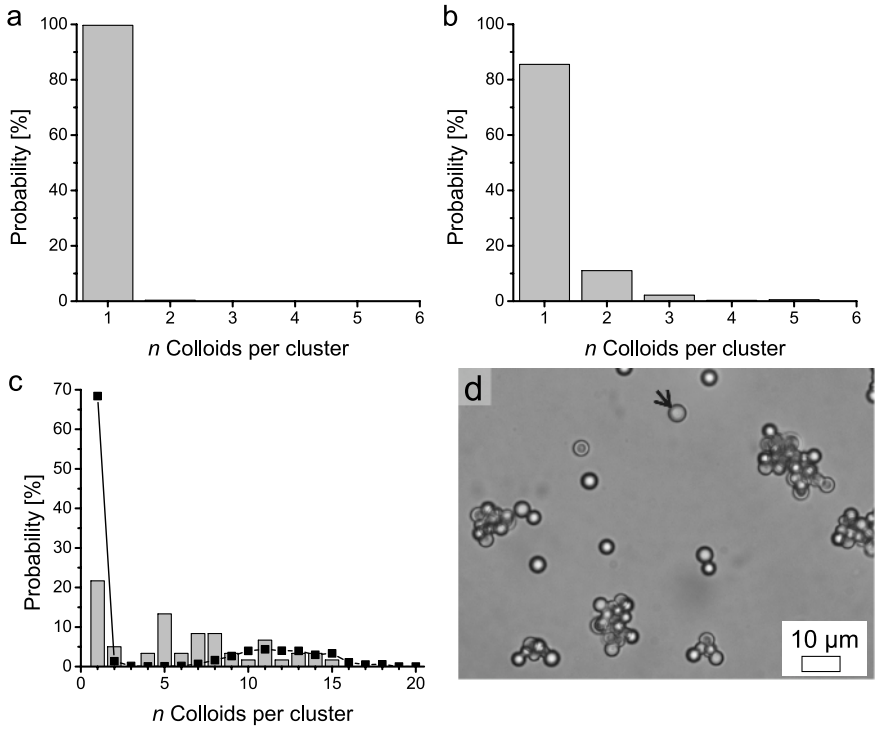

Fig. S6. Cluster size distributions for experiments (bars) and simulations (symbol and line) for dextran polymer with radius $r_p = 8$ nm at concentrations (*A*) $\rho_p = 0.16\rho_{\text{overlap}}$, (*B*) $\rho_p = 0.19\rho_{\text{overlap}}$ and (*C*) $\rho_p = 0.22\rho_{\text{overlap}}$. The experimental cluster size distribution in *C* ranges from $n = 5$ to $n = 15$, whereas simulations show a peak at $n = 10$, probably induced by the long experimental equilibration time due to the short-ranged interactions. (*D*) Transmission light micrograph of sample *C* with $\rho_p = 0.22\rho_{\text{overlap}}$. Data taken 9 d after sample preparation.

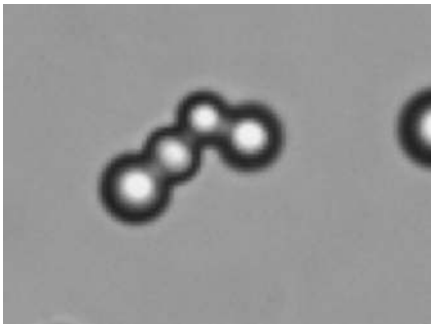

Movie S1. This movie file shows the spontaneous unbinding and binding between two colloids consisting each of one larger rough and one smaller smooth sphere in the presence of polymer ($\rho_p(r = 19\text{ nm}) = 0.38\rho_{\text{overlap}}$). Note that after several binding attempts a bond between the colloids is only established at the end of the movie. The movie was acquired at 30 fr/s and it is displayed at 60 fr/s. (Quicktime, 5 MB)

Movie S1 (MOV)

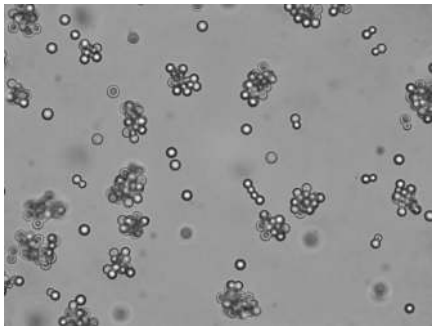

Movie S2. This movie file shows a self-assembled colloidal micelle-like cluster. The colloidal particles assemble in the presence of depletion attraction with their smooth and attractive sides at the interior of the clusters, whereas the rough, non-attractive sides are located at the outside. Despite its larger size, a rough sphere does not take part in the cluster as it does not have a smooth surface. Polymer concentration is $\rho_p(r = 19\ \text{nm}) = 0.38\rho_{\text{overlap}}$. The movie was acquired at 30 fr/s and it is displayed at 30 fr/s (Quicktime, 5 MB)

Movie S2 (MOV)

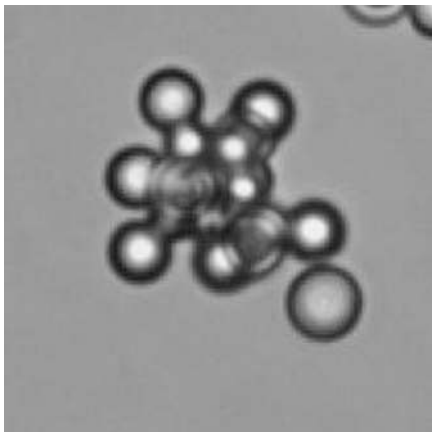

Movie S3. This movie file shows a typical, randomly selected full field of view of our sample containing free colloids as well as colloidal micelles. Polymer concentration is $\rho_p(r = 19\ \text{nm}) = 0.38\rho_{\text{overlap}}$. The movie was acquired at 30 fr/s and it is displayed at 60 fr/s (Quicktime, 2.1 MB)

Movie S3 (MOV)